Transient enhanced diffusion and defect microstructure in high dose, low energy As^+ implanted Si

V. Krishnamoorthy,[a] K. Moller, and K. S. Jones
Department of Materials Science and Engineering, University of Florida, Gainesville, Florida 32611

D. Venables
Department of Materials Science and Engineering, North Carolina State University, Raleigh, North Carolina 27601

J. Jackson and L. Rubin
EATON Corporation, Beverly, Massachusetts 01915

(Received 26 February 1998; accepted for publication 1 September 1998)

(001) CZ silicon wafers were implanted with As^+ at 100 keV to a dose of $1\times10^{15}/cm^2$ in order to produce a continuous amorphous layer to a depth of about 120 nm. Furthermore, the implant condition was such that the peak arsenic concentration was below the arsenic clustering threshold. Subsequently, a second As^+ or Ge^+ implant was performed at 30 keV to doses of $2\times10^{15}/cm^2$, $5\times10^{15}/cm^2$ and $1\times10^{16}/cm^2$, respectively, into the as-implanted samples. All of the samples were annealed at 800 °C for 1 h. The second implant was designed to be contained within the amorphous region created by the initial implant. The second As^+ implant was also designed to provide the additional arsenic needed to exceed the critical concentration for clustering at the projected range. Of the three samples with the dual As^+ implant the clustering threshold was exceeded for the two lower doses while the SiAs precipitation threshold was exceeded at the highest dose. In the case of the dual As^+/Ge^+ implants the clustering and precipitation thresholds were not reached. Since arsenic and germanium are similar in mass the extent of damage created by these implants would be comparable. The implanted and annealed specimens were analyzed using secondary ion mass spectroscopy and transmission electron microscopy. The difference in the defect evolution and the transient-enhanced diffusion of arsenic beyond the end-of-range region between the As^+ and Ge^+ implanted and annealed samples was used to isolate the effects of arsenic clustering and precipitation. The results showed that point defects induced during clustering and/or precipitation did not contribute to the enhanced diffusion of arsenic although these defects did coalesce to form extended defects at the projected range. However, damage beyond the end-of-range region did cause enhanced diffusion of arsenic. © *1998 American Institute of Physics*. [S0021-8979(98)05923-4]

I. INTRODUCTION

The future trend in device technology is toward faster devices with reduced device dimensions. A reduction in device size necessitates the fabrication of ultrashallow junctions. In order to achieve such shallow junctions future processing technologies require low energy implants. In order to achieve high conductivity, highly doped arsenic layers are already widely used in present day *n*-metal–oxide–semiconductor (NMOS) and bipolar transistors. The concentration of arsenic in these layers often exceeds its solid solubility in silicon. This article discusses high dose, low energy implants that are above the amorphization threshold and hence result in a continuous amorphous layer extending from the surface to a certain depth. Such high dose, low energy implants and subsequent anneals give rise to extended defects and anomalous arsenic diffusion that are governed by several factors. Arsenic diffusivity is increased by an increase in either interstitial or vacancy supersaturation. The implant damage beyond the end-of-range region, however, consists predominantly of interstitials. When the amorphous layer regrows during subsequent annealing some of these interstitials cluster and coalesce to form extended defects near the original amorphous/crystalline interface. The remaining interstitials at the end-of-range that do not contribute to extended defect formation may enhance the diffusion of arsenic in this region.[1,2]

When the arsenic concentration exceeds the solid solubility of arsenic in silicon, arsenic clustering and/or precipitation may occur about the projected range of the implant.[3–5] Electrical activation studies[6–8] have attributed arsenic clusters to be the cause of dopant deactivation in silicon. These studies have also determined a critical concentration for arsenic cluster formation, which is a function of the annealing temperature. Previous works on arsenic clustering[6–8] have suggested that these clusters are comprised of two or four arsenic atoms and a vacancy (based on lowest energy configuration). Since a vacancy is used in the formation of these clusters silicon self-interstitials are in turn ejected or left be-

[a]Electronic mail: wish@grove.ufl.edu

hind during cluster formation. This reaction may be illustrated as follows:

$$(As_2)^{2+} + 2e^- \rightarrow (As_2V)^+ + I^-.$$

These interstitials may agglomerate and form extended defects at the projected range. In fact, Parsini *et al.*[7] have shown that these extended defects at the projected range are extrinsic or interstitial in nature. When the arsenic concentration exceeds a critical value monoclinic SiAs precipitates form. Initial stages of SiAs precipitation are not easily detected since the precipitate is coherent with the matrix and does not exert a strain field that is significant enough to be observed by transmission electron microscopy (TEM). Armigliato and Parsini[3] incorporated very large amounts of arsenic into silicon ($\sim 5\times 10^{21}/cm^3$)in order to form large incoherent precipitates (which exert a significant strain field on the matrix and are hence easier to analyze) of SiAs. By evaluating the amount of arsenic contained in these precipitates a concentration of $\sim 3\times 10^{21}/cm^3$(at 800 °C) was suggested as the critical value for SiAs precipitation. It should be noted that this concentration is only a rough estimate. It has been reported that defects at the projected range are absent when the arsenic concentration approaches the critical concentration for precipitation.[9,10] It has been suggested that vacancies released during SiAs precipitation lead to the annihilation of extended defects at the projected range. Three sources of point defects mentioned thus far, namely: the end-of-range damage, arsenic clustering, and arsenic precipitation, may all contribute to the enhanced diffusion of arsenic. However, single implant experiments cannot be used to independently vary the effect of any one of these sources and hence the contribution of any one of these sources towards enhanced arsenic diffusion cannot be independently determined. In this article we report the results from a dual implant experiment specifically designed to isolate the effect of these sources and their contribution towards the enhanced diffusion of arsenic in silicon.

II. EXPERIMENTAL PROCEDURE

Czochralski (001) silicon wafers were implanted with As^+ at room temperature at an energy of 100 keV to a dose of $1\times 10^{15}/cm^2$. The implants were performed at 7° to normal incidence to minimize channeling effects. A continuous amorphous layer from the surface to a depth of 120 nm was created in all of the implanted specimens. A second implant of either As^+ or Ge^+ was performed in the amorphized specimens at an energy of 30 keV to doses of $2\times 10^{15}/cm^2$, $5\times 10^{15}/cm^2$, and $1\times 10^{16}/cm^2$, respectively. All of the samples were furnace annealed at 800 °C for 1 h in flowing nitrogen. Plan-view and cross-sectional transmission electron microscope (PTEM and XTEM) specimens were prepared by standard techniques. These specimens were analyzed using a JEOL 200CX microscope to study the defect microstructure after annealing. The defects were analyzed under a g,$3g$ weak-beam dark field condition using a $g\langle 220\rangle$ reflection. Secondary ion mass spectroscopy (SIMS) analysis was performed using a Perkin Elmer system to determine the arsenic profiles before and after annealing. The analysis was conducted with a 3 keV Cs^+ primary ion beam incident at 60° from the surface normal. The secondary ions analyzed with the quadrupole mass spectrometer were $^{103}AsSi^-$ for the implant species and $^{30}Se^-$ for the matrix species. Relative sensitivity factors for converting secondary ion counts to atomic concentration were derived from As^+ implants of known dose, and the sputter rate was determined from profilometer measurements of the depth of each sputter crater. The estimated relative error in these measurements are ~15% for the atomic concentration and ~2% for the depth scale.

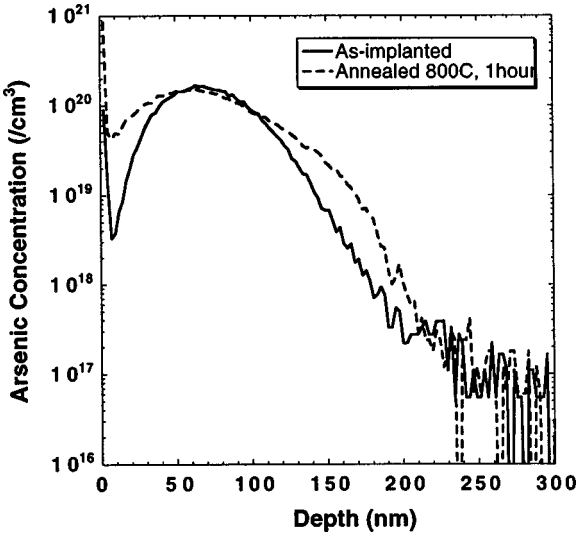

FIG. 1. SIMS profiles of the 100 keV, $1\times 10^{15}/cm^2$ As^+ single implanted control specimen before and after annealing.

III. RESULTS AND DISCUSSION

A. Enhanced arsenic diffusion

In order to determine the extent of arsenic diffusion into silicon the various as-implanted and annealed specimens were analyzed using SIMS. Figure 1 shows the arsenic profiles in the control 100 keV, $1\times 10^{15}/cm^2$ as-implanted and implanted and annealed specimens. The annealed profile clearly shows the absence of a clustered peak at the projected range. In this case one would expect the interstitials created due to the implant cascade at the end-of-range to be the only source of point defects. Therefore the enhanced diffusion in the annealed profile (arsenic should theoretically diffuse only about 1 nm after an 800 °C, 1 h anneal)[11] is due only to the presence of end-of-range damage.

In order to isolate the effects of end-of-range damage and arsenic clustering a second shallow implant of either As^+ or $Ge^+$was performed in the as-implanted control specimen. An example of the as-implanted profiles in these dual implanted specimens is shown in Fig. 2. The dual As^+ implant would result in clustering at the projected range of the second implant if the critical arsenic concentration for clustering is exceeded. Hence, there would be two point defect sources operational in this specimen: one about the peak arsenic concentration (i.e., the projected range of the second implant) and a second at the end-of-range of the initial high

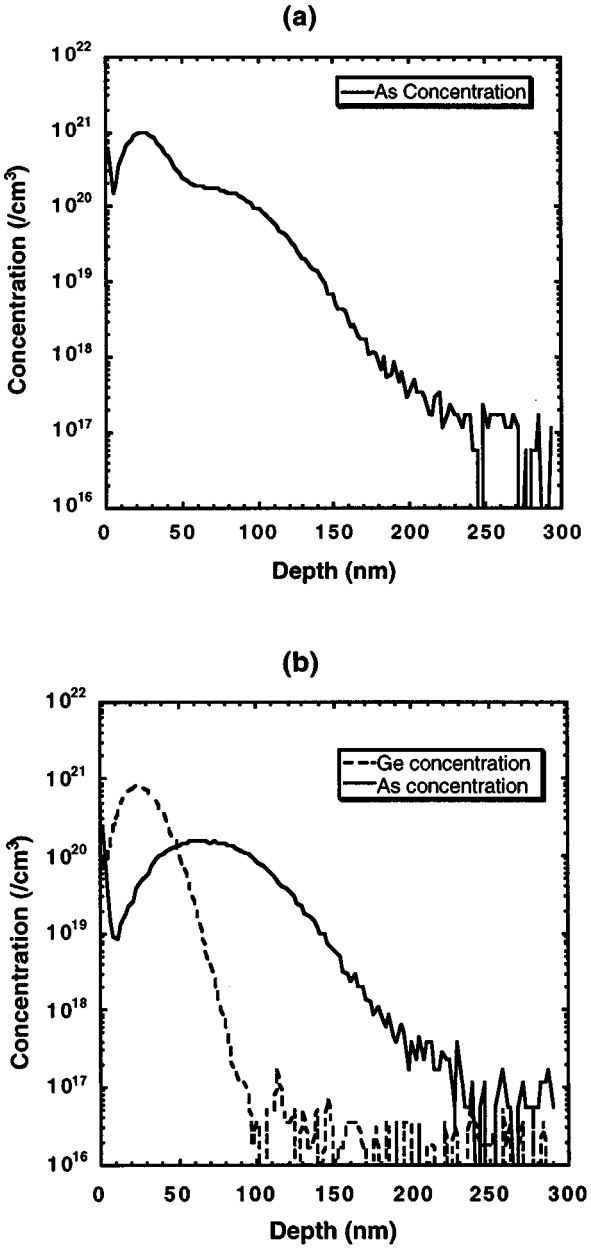

FIG. 2. SIMS profiles of dual as-implanted samples: 100 keV, 1×10^{15}/cm^2 As^+ followed by (a) 30 keV, 2×10^{15}/cm^2As^+ and (b) 30 keV, 2×10^{15}/cm^2 Ge^+.

energy implant. In the dual As^+/Ge^+ implanted specimens only the one point defect source at the end-of-range would be present. Since germanium is close in mass to arsenic the profiles of the second implants (As or Ge) would be very similar. Any additional damage that may be induced by this implant beyond the amorphous/crystalline interface would also be similar. Hence, diffusion of arsenic in the dual As^+/Ge^+ implanted and annealed specimens can be used as a secondary control to estimate the effect of arsenic clustering in the dual As^+ implanted and annealed specimens. Increasing the dose of the second As+ implant would only change the extent of clustering in the dual As^+ implanted specimens. Once a second higher critical arsenic concentration threshold is exceeded one would expect arsenic precipitation to occur at the projected range in the dual As^+ implanted samples.

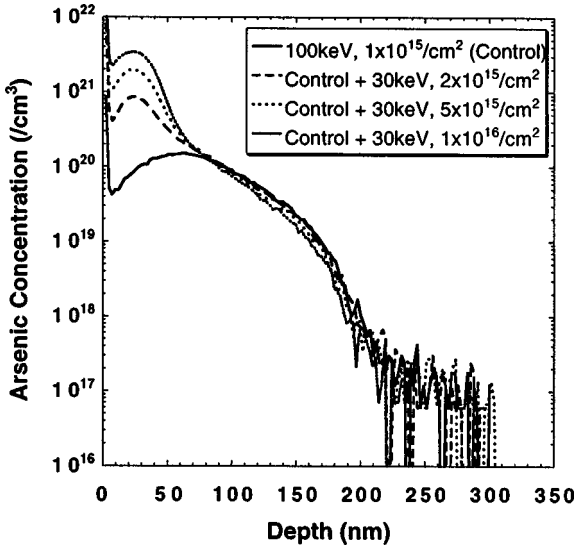

FIG. 3. SIMS profiles of dual As^+ implanted and annealed specimens compared to the single implanted and annealed control specimen. All samples were annealed at 800 °C for 1 h.

Figure 3 shows the arsenic profiles in the variously dual As^+ implanted and annealed samples compared to the control single implanted and annealed specimen. It can be clearly seen that all of the arsenic tails overlap while the peak of the arsenic profile, in the dual As^+ implanted and annealed specimens, remains clustered. Figure 4 shows the diffusion distance of arsenic in all of the dual implanted and annealed samples compared to the single implant and annealed control specimen. The diffusion distance was evaluated at an arsenic concentration of 2×10^{18}/cm^3. Figures 3 and 4 clearly show that the enhancement in arsenic diffusion is similar in all of the samples, suggesting that point defect

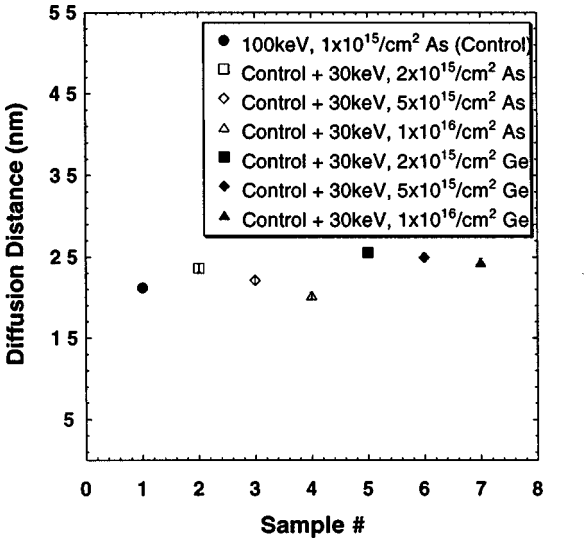

FIG. 4. Diffusion distance of arsenic evaluated at a concentration of 2×10^{18}/cm^3 for the variously implanted specimens after annealing at 800 °C for 1 h.

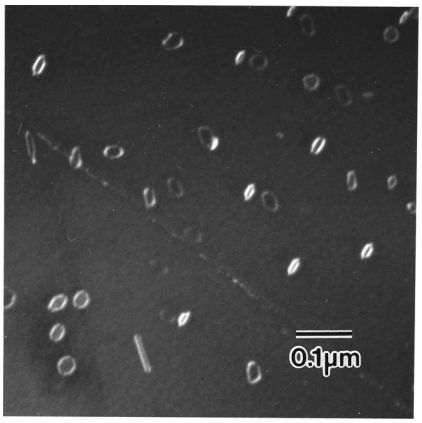

FIG. 5. PTEM micrograph of the 100 keV, $1\times10^{15}/cm^2$ As^+ implanted and annealed control specimen.

sources at the projected range due to arsenic clustering and/or precipitation do not play a significant role in the enhanced diffusion of arsenic.

B. Defect microstructure

The defect microstructure in the variously implanted and annealed specimens was studied using XTEM and PTEM. XTEM analysis of the single As^+ 100 keV, $1\times10^{15}/cm^2$ as-implanted specimen confirmed the presence of a continuous amorphous layer to a depth of about 120 nm. Figure 5 shows a PTEM micrograph from the single implanted and annealed control specimen. The defects are typical of those created during the amorphous layer regrowth and are contained in a single layer at the end-of-range region. The defects consist mainly of dislocation loops along with a few {311} rod shaped defects. Since the peak of the arsenic concentration is below the clustering threshold (as evidenced by the lack of a clustered arsenic peak in Fig. 1) all of the damage in this specimen is due to the amorphizing implant and would occur beyond the amorphous/crystalline interface. Upon annealing the point defects in this region coalesce to form the classical end-of-range defects observed in Fig. 5.

Analysis of the dual As^+ implanted and annealed specimens showed the presence of two layers of defects (Fig. 6) in the two specimens that underwent a second implant to doses of 2×10^{15} and $5\times10^{15}/cm^2$, respectively, while the specimen that was implanted at the highest dose ($1\times10^{16}/cm^2$) showed only a single layer of defects. The dual As^+ implanted and annealed specimens that showed two layers of defects contained one defect layer at the projected range of the second low energy implant and the other at the end-of-range of the initial high energy implant. The single layer of defects in the highest dose dual As^+ implanted and annealed specimen was located at the end-of-range region of the initial high energy implant. All of the dual As^+/Ge^+ implanted and annealed specimens showed only a single layer of defects at the end-of-range region of the initial high energy As^+ implant. Since the addition of germanium would not induce arsenic clustering the presence of only a single layer of defects in the dual As^+/Ge^+ implanted and annealed specimens is not surprising. The two layers of defects observed in

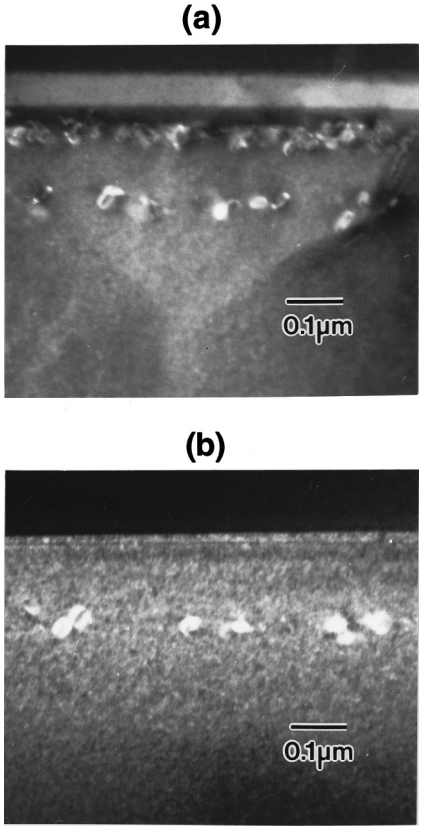

FIG. 6. XTEM micrographs of dual As^+ implanted and annealed specimens. The first implant was performed at 100 keV, $1\times10^{15}/cm^2$ and the second implant was (a) 30 keV, $2\times10^{15}/cm^2$ and (b) $1\times10^{16}/cm^2$. Both specimens were annealed at 800 °C for 1 h.

the dual As^+ implanted and annealed specimens can be attributed to interstitials created at the projected range due to arsenic clustering which may coalesce to form extended defects in this region and end-of-range damage due to the initial amorphizing implant agglomerating to form extended defects at the end-of-range. In the case of the highest dose dual As^+ implanted and annealed specimen, arsenic precipitation could be occurring at the projected range that may suppress interstitial generation and hence extend defect formation in this region.

Qualitative and quantitative PTEM analyses were performed on all of the dual implanted and annealed specimens. Figure 7 shows PTEM micrographs from the various dual implanted and annealed specimens. It can be clearly seen that the specimens that contain two layers of defects show a significantly higher number of defects than those that have a single layer of end-of-range defects. The increase in defect density clearly suggests that interstitials are ejected during arsenic clustering. The total number of atoms associated with the defects (whether the defects were contained in one or two layers) was evaluated by assuming that the dislocation loops lie on {111} planes and are circular and that the {311} defects are rod shaped and elongated along ⟨110⟩ directions. The results of this analysis are plotted in Fig. 8. The total number of atoms contained by defects is a measure of the total number of interstitials that collapsed to form extended defects both at the projected range of the second implant and the

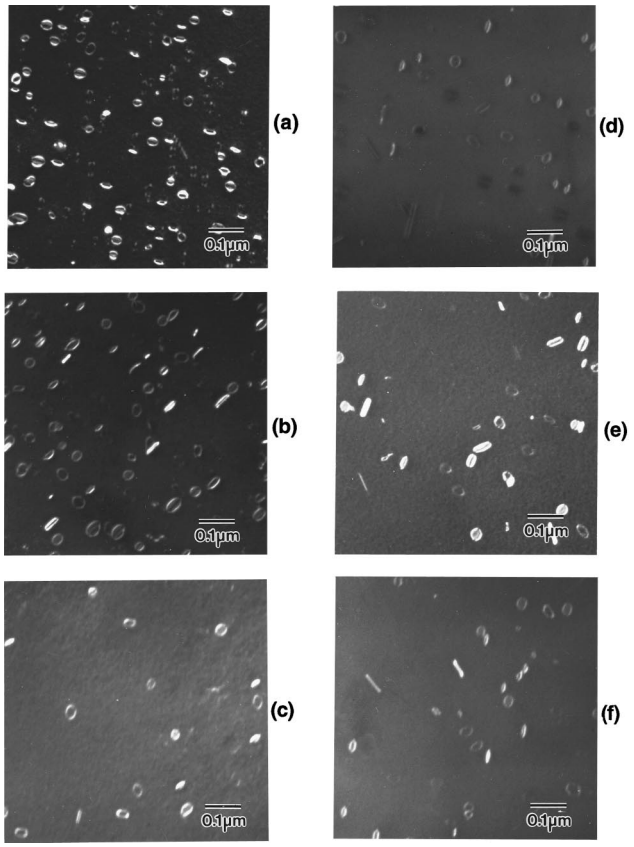

FIG. 7. PTEM micrographs of dual implant and annealed specimens. All specimens were annealed at 800 °C for 1 h. The first implant was a 100 keV, 1×10^{15}/cm^2 As^+ implant while the second implant was as follows: (a) 30 keV, 2×10^{15}/cm^2 As^+, (b) 30 keV, 5×10^{15}/cm^2 As^+, (c) 30 keV, 1×10^{16}/cm^2 As^+, (d) 30 keV, 2×10^{15}/cm^2 Ge^+, (e) 30 keV, 5×10^{15}/cm^2 Ge^+, and (f) 30 keV, 1×10^{16}/cm^2 Ge^+.

end-of-range of the initial high energy implant. It can be seen that this number remains the same in all the dual As^+/Ge^+ implants and is comparable to that in the control single implant specimen. This similarity implies that the second implant was contained within the amorphous region created by the first implant and hence no excess damage was introduced into the end-of-range region by the second low energy implant.

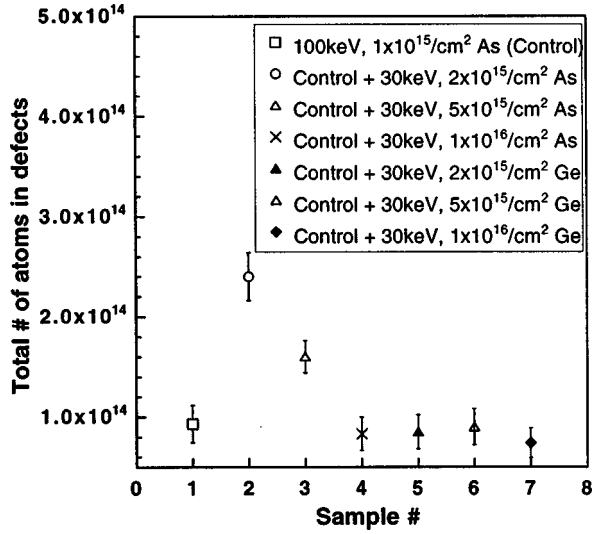

FIG. 8. A plot of the total number of atoms associated with defects in the variously implanted specimens after annealing at 800 °C for 1 h.

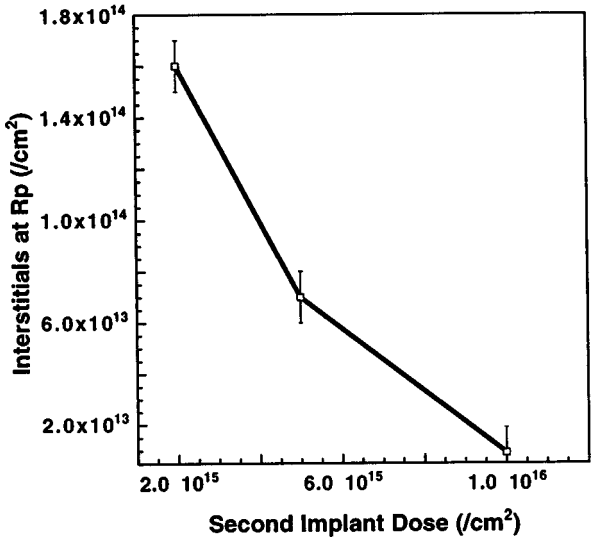

FIG. 9. A plot of the estimated net number of interstitials remaining as a function of the dose of the second As^+ implant.

If we assume that the implant damage introduced in the dual As^+ implants is similar to that in comparable dual As^+/Ge^+ implants then by taking the difference in the number of atoms contained by defects between the two we can estimate the number of point defects introduced during arsenic clustering and/or precipitation. This assumption is valid since the masses of arsenic and germanium are comparable. A plot of the number of atoms associated with defects at the projected range after dual As^+ implant and anneals is shown in Fig. 9. It can clearly be seen that most interstitials are generated after a 30 keV, 2×10^{15}/cm^2 second implant and anneal, suggesting that this specimen had the most arsenic clusters. Increasing the second arsenic implant dose by 2.5 and 5 times reduced the interstitial content by about 2 and 10 times, respectively. These data suggest that SiAs precipitation is already induced after implantation at 5×10^{15}/cm^2. The formation of SiAs precipitates may be suppressing arsenic cluster formation and hence reducing the number of interstitials ejected. It is also possible that precipitation occurs sequentially after arsenic cluster formation, in which case the vacancies associated with arsenic clusters may be released. These vacancies would, in turn, recombine with interstitials and reduce the number of interstitials available to form extended defects. It is not possible at this point to distinguish between these two probable mechanisms, although it is clear that the transition between arsenic clustering and precipitation is not abrupt.

IV. CONCLUSIONS

The results from this study clearly show that in the case of low energy, high dose amorphizing implants, point defects that may be induced by arsenic clustering and/or precipitation do not affect the enhanced diffusion of arsenic beyond

the end-of-range. Also, analysis of the defect microstructure revealed that the transition between arsenic clustering and SiAs precipitation is not abrupt and that arsenic clusters and SiAs precipitates (although not directly observed) can coexist although the exact mechanism by which the SiAs precipitates form is not clear.

[1] D. Nobili, S. Solmi, A. Parsini, M. Derdour, A. Armigliato, and L. Moro, Phys. Rev. B **49**, 2477 (1994).
[2] Y. Kim, H. Z. Massoud, and R. B. Fair, J. Electron. Mater. **18**, 143 (1989).
[3] A. Armigliato and A. Parsini, J. Mater. Res. **6**, 1701 (1991).
[4] A. Armigliato, A. Parsini, M. Derdour, P. Lazzari, L. Moro, D. Nobili, and S. Solmi, Solid State Phenom. **19&20**, 393 (1991).
[5] A. Parsini, D. Nobili, A. Armigliato, M. Derdour, L. Moro, and S. Solmi, Appl. Phys. A: Solids Surf. **54**, 221 (1992).
[6] J. Said, H. Jaouen, G. Ghibaudo, and I. Stoemenos, Phys. Status Solidi A **117**, 99 (1990).
[7] A. Parsini, A. Bourret, A. Armagliato, M. Servidori, S. Solmi, R. Fabbri, J. R. Regnard, and J. L. Allain, J. Appl. Phys. **67**, 2320 (1990).
[8] P. M. Rousseau, P. B. Griffin, and J. D. Plummer, Appl. Phys. Lett. **65**, 578 (1994).
[9] S. N. Hsu and L. J. Chen, Nucl. Instrum. Methods Phys. Res. B **55**, 620 (1991).
[10] S. N. Hsu and L. J. Chen, Appl. Phys. Lett. **55**, 2304 (1989).
[11] J. W. Mayer and S. S. Lau, *Electronic Materials Science: For Integrated Circuits in Si and GaAs* (McMillan, New York, 1990).